Laser-assisted Auger decay as free-free transitions in a high-intensity laser field

J.M. Schins, P. Breger, and P. Agostini

Service des Photons, Atomes et Molecules, Centre d'Etudes de Saclay, 91191 Gif-sur-Yvette, France

R.C. Constantinescu and H.G. Muller

FOM-Institute for Atomic and Molecular Physics, Kruislaan 407, 1098 SJ Amsterdam, The Netherlands

G. Grillon, A. Antonetti, and A. Mysyrowicz

Laboratoire d'Optique Appliquée, Ecole Polytechnique–Ecole Nationale Supérieure de Techniques Avancées, 91120 Palaiseau, France

We investigate the effect of an intense optical field on the energies of electrons ejected in an Auger process. To this end, part of a subpicosecond, infrared laser beam is focused onto a metal target to produce subpicosecond, broadband x radiation. Electrons resulting from the x-ray-induced LMM Auger transition in argon are detected in a time-of-flight electron spectrometer. The other part of the infrared laser beam is directly focused onto the argon atoms. When the x-ray-induced Auger transition takes place in the presence of the intense dressing beam, sidebands appear around the Auger peaks in the electron spectrum, corresponding to absorption or emission of photons from the dressing field. The magnitude of the sidebands is studied as a function of dressing field intensity. Good quantitative agreement with quantum-mechanical theory is reported.

PACS number(s): 32.80.Hd, 32.80.Wr

I. INTRODUCTION

The past decade has witnessed a spectacular rise of electron spectroscopy of optical multiphoton ionization processes, yielding valuable information concerning the behavior of atoms in intense radiation fields. Especially above-threshold ionization, the absorption of excess photons during multiphoton ionization (MPI), has received considerable attention [1]. This process is sometimes described theoretically in terms of an ionization step *followed* by absorption of excess photons by the free electron. A major problem in applying this scheme is that normally, the ionizing laser drives both bound-free and free-free transitions in atoms. In multiphoton ionization the bound-free part of the ionization process is strongly influenced by resonances with (Stark-shifted) atomic states in intermediate steps [2]. This considerably complicates the study of the accompanying free-free transitions.

An attempt to disentangle bound-free from free-free processes was undertaken by Muller *et al.* in a two-color experiment [3]. In that experiment, the target gas was ionized in a multiphoton transition using a high-frequency ultraviolet (uv) laser at relatively low intensities, while a low-frequency infrared (ir) laser induced the subsequent free-free transitions. The ionization caused by the low-frequency laser could be kept negligibly small because of the large number of ir photons needed to overcome the ionization potential of the atom. Yet the interpretation of this two-color experiment remained ambiguous because the bound-free step still required three uv photons.

Of course, single-photon ionization with a hard photon would considerably simplify the description of the two-color ionization process [4]. In that case the first (bound-free) step of the ionization process would be completely insensitive to atomic resonances. The influence of the atomic structure on the process would then be limited to target-dressing effects, which are small except close to the ionization threshold [5].

In the experiment described in this paper, we have chosen a slightly different approach to realize a simple initial ionization step: We make use of Auger decay rather than narrow-band photoionization. This has the advantage that we can excite the atoms with broadband radiation. Electrons resulting from an Auger process have a well defined energy, determined by the energy difference between two bound states: the singly charged ion excited state and the doubly charged ion ground state. To prepare the target atoms in an excited state that is susceptible to Auger decay, we thus can use broadband x radiation to eject an inner-shell electron from a neutral argon atom. In this way we obtain a source of energetic electrons that can be subjected to a low-frequency laser in order to study free-free transitions [6].

A scheme showing the levels participating in the present experiment is shown in Fig. 1. In its ground state, argon has the configuration $1s^2 2s^2 2p^6 3s^2 3p^6$. The core-hole state $Ar^{+*}(2p^5 3s^2 3p^6)$ can be reached with photons having energies higher than 255 eV. The excess energy is absorbed by the ejected photoelectron. The core-hole state is very short lived (the linewidth is equal to 0.1 eV [7], corresponding to a lifetime of 6 fs) and decays, by emission of an Auger electron, to the ground state of the
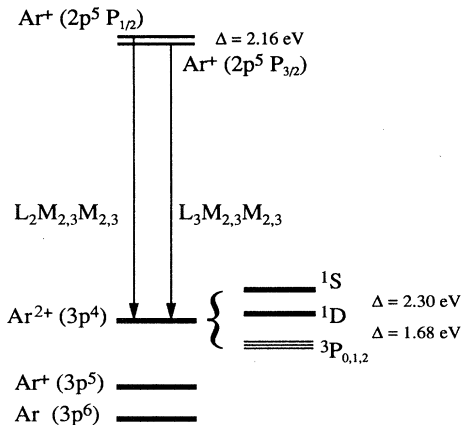
FIG. 1. Level scheme of argon, including only the states that intervene in the present experiment. Pulsed, broadband x radiation excites argon from its ground state to beyond the core-hole states $\text{Ar}^+(2p^5)$, the photoelectron carrying away any excess energy. Auger transitions to the ground state of the doubly excited species yield different lines due to the fine-structure of the upper and lower states. The fine-structure splittings are given in the figure. The energy separating the members of the triplet of $\text{Ar}^{2+}(3p^4)$ is less than the lifetime broadening of the Auger transitions.

doubly ionized species $\text{Ar}^{2+}(3p^4)$. The $3p^4$ configuration gives rise to the ^1S, ^1D, and $^3P_{0,1,2}$ states. Since the upper state Ar^{+*} is a doublet $(^2P_{1/2,3/2})$, six lines should be seen.

In the next section we present the experimental set-up and show that the experimental resolution is such that the six Auger lines merge into four peaks. When subjected to a low-frequency, high-intensity laser field, the experimental spectrum is profoundly modified (Sec. III). A deconvolution of the modified spectrum with the original spectrum (taken without the dressing field) shows that the modification of the spectra really results in sidebands on each Auger transition. In Sec. IV the quantum-mechanical predictions are compared to our experimental data.

II. EXPERIMENT

Figure 2 shows a schematic of the experimental set-up. The output pulse of a self-mode-locked Ti:S laser is stretched to 400 ps and amplified in two stages. After recompression, 40-mJ pulses of 150 fs at 800 nm (infrared) with a repetition rate of 10 Hz and a near-Gaussian spatial profile of 10 mm full width at half maximum [8] are available.

A beam splitter divides the incoming beam into two branches. One of the beams provides the strong optical field, the other one produces the x rays. The former, to be called the "dressing" beam, is led through a variable delay and passed through a tilted multilayer dielectric mirror (coated for 800 nm at 45°). Slight rotation of this mirror (between 10° and 20° angle of incidence) allows for adjustment of the beam intensity from zero to maxi-
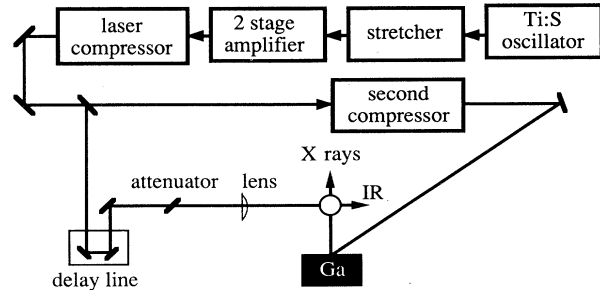

FIG. 2. Schematic of the experimental setup. An amplified Ti:S laser delivers 40-mJ pulses at 800 nm. According to the setting of the laser compressor these pulses have a duration variable from 150 fs to 8 ps. A beam splitter divides the laser beam into two. One part of the beam passes through a second compressor before it is focused on the gallium target. Another part of the beam is led through a delay line and attenuator before being focused in the interaction region. The plasma irradiates x radiation, which crosses the ir beam at a right angle in the interaction region.

mum while hardly affecting the other beam parameters. The beam is subsequently focused into an electron spectrometer by means of a planospherical lens ($f = 2m$). In the focus it crosses the x-ray beam at right angles. In order to get good temporal overlap with the x-ray pulse, the laser compressor was adjusted in order to chirp out the pulses to a duration of 2.5 ps. The pulse energy is monitored by recording the reflection from the focusing lens on a photodiode.

The second beam leaving the beam splitter is used to produce the x rays by pumping a plasma. It is passed through a single-pass grating compressor (marked as "second compressor" in Fig. 2) to allow for independent variation of the pulse duration of the x-ray pump and dressing beams. By means of a lens of 200 mm focal length, the pump beam is focused onto a gallium target, thereby creating a plasma burst, which emits subpicosecond broadband x radiation [6].

The time-of-flight electron spectrometer is of the magnetic bottle type, designed for collection over a 2π sr solid angle [9]. In such a spectrometer the electrons are created in a high magnetic field (about 0.9 T), parallelized due to their transiting to a low magnetic field (1.5 mT), and detected after having traversed a distance of 1.50 m, thus enabling a time-of-flight measurement. The detector consists of two microchannel plates and is connected to a digital sampling scope.

The polarization of the dressing field coincides with the magnetic field lines of the spectrometer and is perpendicular to the x-ray beam. The interaction region of the spectrometer is shown in more detail in Fig. 3. An aperture placed on top of the right-hand magnetic pole piece limits the volume of acceptance of the electron spectrometer to a cylinder of 2 mm length along the spectrometer axis and of 0.25 mm diameter. Due to the high magnetic field directed along the spectrometer axis, the electrons spiral within the cylinder of acceptance (200-eV electrons have a cyclotron radius of about 50 μm) until they reach the inner part of the right-hand pole
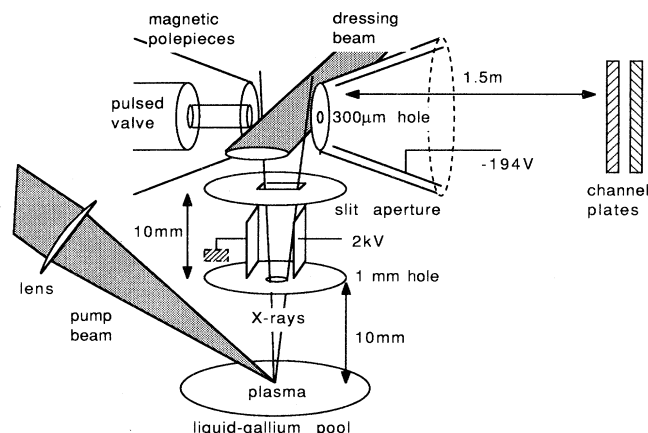
FIG. 3. Schematic of the interaction region. The volume of sensitivity is located in between the two magnetic cones, its diameter being determined by the diaphragm in the right-hand cone (0.25 mm). The x-ray beam originates from a laser-induced plasma on the gallium surface, is led through a couple of diaphragms, and illuminates part of the volume of sensitivity. Two deflection plates allow for removal of ions and electrons from the plasma-emitted beam. The electron detector is located at the end of the time-of-flight section, to which a retarding voltage is applied.

piece. The electron velocities are parallelized in the region of strong magnetic field gradient, before entering the time-of-flight tube. In order to get good resolution of the spectrometer at energies above 20 eV, the electrons are decelerated in the same region, i.e., inside the right-hand pole piece. To this end, a conical electrode was inserted in the magnetic pole piece and set to a constant negative potential. In this way, the most critical stage of the parallelization takes place at low kinetic energy of the electrons. Sufficient resolution (0.5 eV) around 200 eV was obtained by retarding the electrons to an energy of about 5 eV. A pulsed valve was positioned behind the opposite pole piece, at the left-hand side in Fig. 3. This allows for high local pressures (10^{-1} Torr) of the target gas, synchronized with the laser pulses, while maintaining an acceptable background pressure (10^{-6} Torr). The small hole on the right-hand pole piece acts as a pump resistance such that the pressure in the time-of-flight part could be kept at 10^{-9} Torr.

The plasma is created 33 mm below the spectrometer axis. The gallium target is heated to 40° to keep it liquid. This makes the surface self-regenerating, while the low vapor pressure of gallium (below 10^{-9} Torr) is compatible with our high-vacuum system.

The x-ray emission is collimated by two apertures separated by 10 mm that determine an axis perpendicular to both the dressing beam and the spectrometer axis. Between the apertures two deflection plates are mounted. A constant potential difference (2 kV) prevents most of the charged debris leaving the plasma from reaching the acceptance volume. This reduces the "dark" counts generated by the plasma debris when no target gas is fed into the spectrometer by 95%. Introduction of the target gas leads to copious electron production below 10 eV, which is blocked by the retarding voltage.

The crucial requirement of this experiment is the overlap between the x-ray and dressing beams on the spectrometer axis. The spatial overlap is achieved by tilting the focusing lens by 30° such as to create an astigmatic focus, elongated along the magnetic field lines, which measures 2 mm in that direction. For alignment purpose, the laser compressor is set to 0.5 ps. This provides enough intensity in the laser focus to ionize xenon by MPI and the overlap of the dressing beam with the spectrometer cylinder of sensitivity is optimized by maximizing this MPI signal. The size of the astigmatic focus is measured in two steps. The size of its short axis (0.2 mm) could be measured by monitoring the MPI signal as a function of the vertical focus position. The long axis (2 mm) is measured by taking an image of the focus with a charge coupled device camera.

In order to obtain an approximately constant (within a factor of 2) intensity profile throughout the volume of sensitivity, the lens is positioned such that the astigmatic focus falls about 10 mm in front of this volume of sensitivity. Accordingly, the dimension of the optical dressing beam perpendicular to the magnetic field lines is about 0.5 mm (twice the diameter of the cylinder of acceptance), while leaving the long axis (2 mm) unmodified.

The absolute intensities have been estimated from the pulse energy, the duration, and the size of the illuminated spot (1 mm^2) and are subject to large errors. The relative values, though, are reliable to within 1%, following directly from the monitored photodiode signal. The intensity of the dressing beam is limited to 1 TW/cm^2 and no photoelectrons are detected with the optical pulse only.

Besides spatial overlap between the x-ray and dressing beams, temporal overlap is needed as well. In order to allow for a roughly constant dressing intensity during the x-ray pulse, the pulse duration of the plasma-pumping beam (0.5 ps) is made much shorter than the dressing pulse (2.5 ps).

The x rays are collimated by two small apertures to closely match them to the sensitivity volume. A slit measuring 1.5 × 0.4 mm^2 positioned 10 mm below the spectrometer axis and a 1-mm hole 10 mm below it are used to this end. It was found that a larger slit increased the Auger signal but yielded no overlap signal (sidebands).

Due to the small aperture separating the interaction region from the time-of-flight section (see Fig. 3) the spectra are in principle slightly distorted: electrons created very close to the boundary of the cylinder of sensitivity (see Sec. II) are more likely to pass through the aperture if their velocity is aligned with the magnetic field of the spectrometer. This effect was calculated to be smaller than 5% and is neglected in the following.

With 2 mJ of energy per pulse in the plasma-pumping branch, the intensity on the target is about 10^{16} W/cm^2. Below 1.5 mJ pumping energy no x-radiation above 255 eV is produced, as can be deduced from the disappearance of the Auger signal from argon atoms. The deposition of debris on the window transmitting the pump-beam is the main drawback of this method. It limits the pumping energy on the target to about 2 mJ per pulse.

III. RESULTS

The pressure of the target gas in the sensitivity region of the electron spectrometer was estimated on the basis of the mean background pressure (10^{-5} Torr), the measured duration of the valve opening time (1 ms), the valve backing pressure (5 atm), and the mean distance of the sensitivity region to the valve. On the basis of the mean number of electrons recorded per laser shot (13), the estimated target gas pressure at the moment of the laser pulse (10^{-1} Torr), and the photoionization cross section of about 3 Mb in an 100 eV energy range around 300 eV, one can estimate the conversion efficiency of our plasma x-ray source. On assuming a cosine-distributed x-ray emission cone we find an energy conversion efficiency of 10^{-5} for x-ray photons in the above-mentioned range, integrated over 2π solid angle. Since we pumped the plasma with 2 mJ, this efficiency implies the creation of about 10^9 photons per laser shot.

When no optical radiation is present, the broadband x-radiation emitted from the plasma source excites the argon atoms in many different ways, some resulting in ionization. The resulting electron spectrum is shown in Fig. 4 for the energy range from 0 to 220 eV. In order to get a good resolution over such a large energy range, the data in Fig. 4 were accumulated in seven separate runs, each one having a different retarding voltage. At energies below 30 eV many lines can be seen that are probably due to autoionizing states decaying to the Ar^+ ground and first excited states [10].

The three structures at highest energies (marked A, B, and C in Fig. 4) correspond to $L_{2,3}MM$ Auger transitions. In all three cases the inner-shell electron is a $2p$ electron (L_{23}); for structure C, two $3p$ electrons are involved in the Auger process ($M_{2,3}M_{2,3}$), for A, two $3s$ electrons (M_1M_1), and for B, a $3p$ and a $3s$ electron ($M_1M_{2,3}$).

The present experiment is concerned with structure C, the $L_{2,3}$ $M_{2,3}$ $M_{2,3}$ transition. A spectrum corresponding to this transition is shown in Fig. 5 (bold curve). Given the resolution of our spectrometer, from the six Auger lines predicted in the introduction, only four peaks are
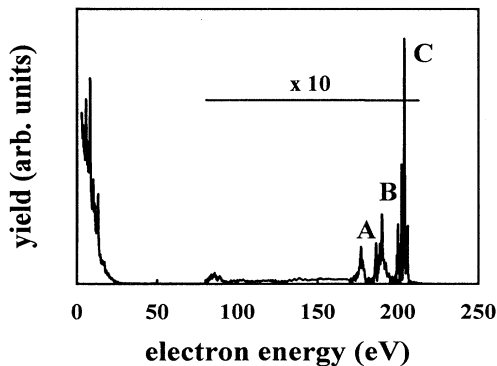

FIG. 4. Argon photoelectron spectrum for broadband x radiation as irradiated by a laser-generated plasma. The three structures marked A, B, and C originate from the $3s$-$3s$, the $3s$-$3p$, and the $3p$-$3p$ Auger transitions, respectively.
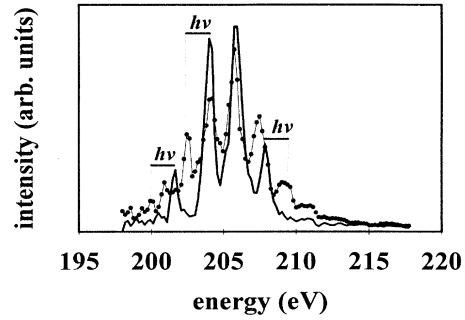

FIG. 5. The thin curve shows a spectrum of the $L_{2,3}M_{2,3}M_{2,3}$ Auger transition in argon. The bold curve shows a spectrum of the same transition in the presence of an intense dressing field (145 GW/cm^2). Two-sided arrows mark the energy of the dressing photon (1.55 eV).

resolvable. A typical run requires accumulation over 4000 laser shots, with a mean counting rate of 13 per laser shot.

The four-peak Auger structure is heavily modified by the presence of the dressing beam: The spectrum shown in Fig. 5 (thin curve) was taken with a dressing beam intensity of 150 GW/cm^2. The new peaks due to the presence of the dressing field are readily identified. A two-sided arrow marks the energy of the infrared dressing photon (1.55 eV), showing that the sidebands are indeed separated by a photon quantum from their mother peak.

As we will now see, this is even more visible after deconvolution of the raw spectra with the unmodified spectrum (i.e., the spectrum in the absence of the dressing field). The dressed electron spectra are assumed to arise from a convolution of the unmodified spectrum with some "sideband function." Since a convolution of two functions corresponds to multiplication of their Fourier transforms, we have

$$D(k) = S(k)A(k) + N(k), \tag{1}$$

with $D(k), S(k), A(k)$, and $N(k)$ the Fourier-transformed dressed spectrum, the sideband spectrum (i.e., the deconvoluted spectrum), the unmodified spectrum (i.e., the Auger spectrum), and the noise spectrum, respectively. The argument k corresponds to the reciprocal energy in Fourier space. Straightforward division of the data $D(k)$ by the bare Auger spectrum $A(k)$ leads to excessive blow up of the noise in those regions of k space where $A(k)$ vanishes. To regularize the deconvolution problem, an additional noise function $N(k)$ is introduced that satisfies Eq. (1) while minimizing the quantity

$$\int \left(w|S|^2 + |N|^2\right) dk. \tag{2}$$

This is achieved with

$$S(k) = D(k)A^*(k)/[|A(k)|^2 + w], \tag{3}$$

where the asterisk represents the complex conjugate. The constant w weighs the importance of the noise with respect to the sideband spectrum in the minimization problem: for noiseless spectra $w = 0$ and ordinary deconvolution results. For the present spectra, the most satisfac-

tory deconvolutions were obtained on using a numerical value w, which equals 1.6×10^{-2} times the mean value of $|A(k)|^2$.

An example of a deconvoluted energy spectrum is shown in Fig. 6 for a dressing field intensity of 436 GW/cm^2. From this example it is evident that the dressed spectrum is indeed a convolution of some sideband spectrum with the unmodified spectrum, such that the sideband spectrum consists of a series of peaks separated by the photon energy. However, all spectra deconvoluted using the above-mentioned algorithm suffer a common disease: they seem to be superimposed on an oscillatory structure, which can be seen from the behavior of the minima of the sideband spectrum in Fig. 6. This oscillatory structure is a consequence of the undressed Auger spectrum having two peaks of approximately the same height, which makes $A(k)$ nearly vanish at the k value corresponding to the peak spacing. This deconvolution procedure extracts the maximum amount of information from the raw data, without using any *a priori* knowledge concerning the functional form of the spectra. For accurate comparison with theory this is unfortunately not sufficient because of the problem with the oscillating base line.

However, once we established that the measured spectrum is the convolution between the unmodified spectrum and a discrete set of peaks separated by the photon energy, we can use this knowledge and the magnitude of these peaks as fit parameters. They are adjusted such that optimal agreement of the convolution with the measured spectrum is obtained. Figure 7 shows the result of this procedure, for example, spectra taken at two dressing field intensities. The thin curve represents the experimental result (the dressed spectrum), the bold one the fitted result. In both cases the agreement decreases at the low-energy side of the electron spectrum, where the experimental resolution is best. This paradox is a consequence of a convolution, which implies shifts in the energy domain, not being able to cope with an energy-dependent instrument resolution.
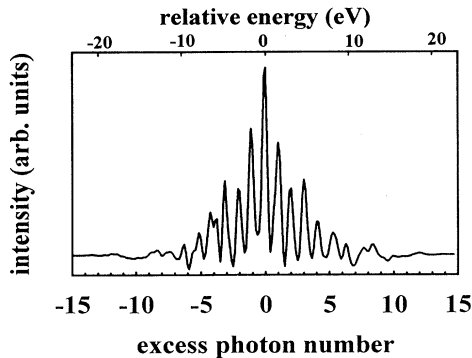

FIG. 6. Deconvoluted energy spectrum for a dressing field intensity of 436 GW/cm^2. The distance between two successive maxima can be seen to equal the photon energy (1.55 eV).
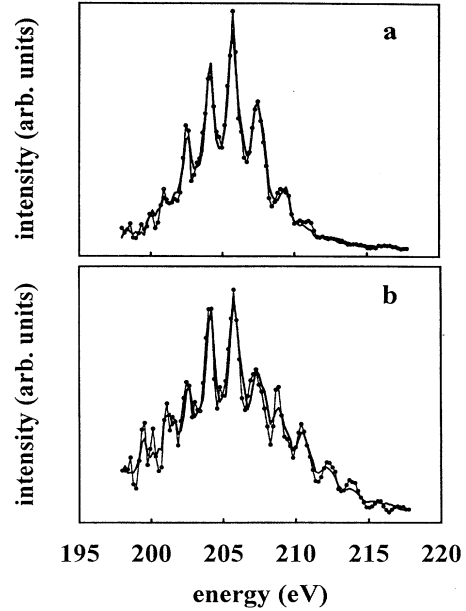

FIG. 7. Two experimental spectra (solid curve) and the corresponding optimized convolutions (dotted curve) at dressing field intensities of (a) 145 GW/cm^2 and (b) 436 GW/cm^2.

IV. DISCUSSION

Theoretical work concerning laser-assisted Auger decay (LAAD) has been published recently by Fiordilino, Zangara, and Ferrante [11]. In the following, some basic steps are recalled that lead to an explicit expression for the sideband strength as a function of dressing field intensity. A theoretical description of LAAD must evidently take into account the non-perturbative nature of the free-free transitions. However, the first step of the process, the Auger decay itself, can be described by ordinary perturbation theory. Auger decay is just a form of autoionization, where the Coulomb repulsion between electrons eventually leads to concentration of enough energy in one of the electrons to enable ionization. In an independent-electron model (e.g., a Hartree-Fock description) Auger decay cannot occur.

The S-matrix expression for a transition from the initial state i to the final state f can be written as

$$(S - 1)_{if} = -i \int \langle \Psi_i | H_I | \Phi_f \rangle \, dt, \qquad (4)$$

where Ψ_i describes the evolution of the initial state under the full Hamiltonian H, Φ_f describes the free evolution of the final state under a zeroth-order Hamiltonian H_0, and H_I is the interaction defined as $H - H_0$. If H_I is a small perturbation, it is sufficient to include only terms first order in H_I. This is achieved by replacing Ψ_i by Φ_i, the free evolution of the initial state.

The present description does not include the initial excitation of the core-hole state by the x-ray photon. The initial state Ψ_i describes therefore the Ar^{+*} core-hole state. Our experiments on LAAD are largely beyond the

perturbative limit as far as the low-frequency laser inter-
action is concerned, which, as a consequence, has to be
included in H_0. Only the interelectronic Coulomb inter-
action occurs in H_I, which can be taken as the difference
between the exact electronic repulsion

$$C = \sum_{i,j} 1/r_{ij} \qquad (5)$$

and the average interaction

$$V = \sum_i V_C(r_i) - V_X(r_i), \qquad (6)$$

which is already taken into account in the (Hartree-Fock)
zeroth-order description. In this expression, V_C and V_X
denote the Coulomb and exchange potentials, respec-
tively. The free evolution is then generated by

$$H_0 = \frac{1}{2}(p - A)^2 + V \qquad (7)$$

and in principle both initial and final states should have
this evolution (p and A stand for the momentum and
vector-potential operators). In the LAAD case, the ini-
tial state is strongly bound and hardly affected by the
laser field. This justifies replacing Φ_i by the unper-
turbed (Hartree-Fock) ground state Φ_{HF}, evolving under
$H_0' = \frac{1}{2}p^2 + V$. The final state, on the other hand, has
a very high kinetic energy and is hardly affected by the
presence of the atomic potential. Thus we replace it by
a *plane wave* evolving under $H_0'' = \frac{1}{2}(p - A)^2$.

These two approximations are just the ones underly-
ing the *classical* description of ionization in a strong laser
field known as Simpleman's theory [12], namely, the cre-
ation of an electron in a way independent of the laser
field, followed by classical motion of the electron as if
it were independent of the ion. Simpleman's theory has
been very successful in explaining the energy range over
which the LAAD peaks extend [6]. Being a classical the-
ory, though, it is of course incapable of predicting the
exact peak structure of the LAAD spectrum.

The quantum-mechanical expression for the LAAD
amplitudes now becomes, with $|\Phi_{\mathrm{HF}}\rangle$ and $|k\rangle$, the ap-
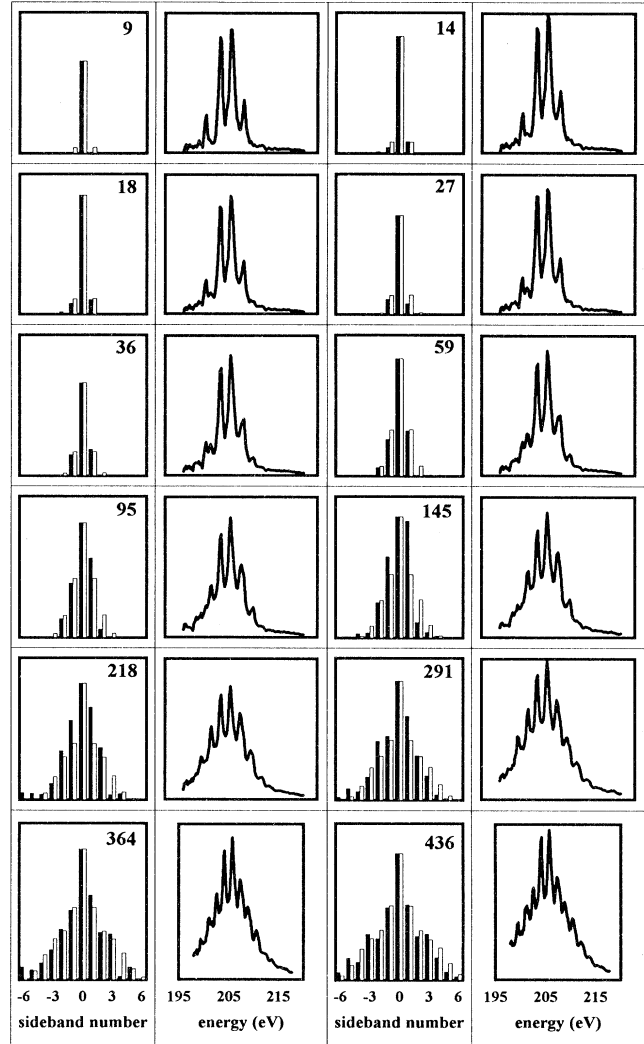proximated initial and final states

FIG. 8. Comparison of experimental (black bars) and the-
oretical (white bars) sideband functions for 12 different values
of the dressing field intensity, in units of $\mathrm{GW/cm^2}$. To the
right of each histogram the raw data are shown for the cor-
responding field intensity. The vertical intensity scales are
omitted, since all bars are normalized on the central, $n = 0$
sideband.

$$(S - 1)_{if} = -i \int e^{iE_{\mathrm{HF}}t'} \left\langle \Phi_{\mathrm{HF}} | C - V | \exp\left(-i \int_{-\infty}^{t'} \frac{1}{2}[p - A(t)]^2 d\right) k \right\rangle dt', \qquad (8)$$

yielding

$$(S - 1)_{if} = -i\langle \Phi_{\mathrm{HF}} | C - V | k \rangle$$
$$\times \int e^{iE_{\mathrm{HF}}t'} e^{-i(\frac{1}{2}k^2 + \frac{1}{4}A^2)t'}$$
$$\times e^{i(\frac{kA}{\omega}\sin\omega t' - \frac{A^2}{8\omega}\sin 2\omega t')} dt', \qquad (9)$$

where we used $A(t) = A\cos\omega t$. This expression is very
similar to that obtained by Becker *et al.* [13], but differs

by the use of the electron source $(C - V)|\Phi_{\mathrm{HF}}\rangle$ instead
of a δ function. The results are very similar, though,
since in the LAAD case the final states have very similar
energy. As a consequence the spatial part of the matrix
element becomes nearly independent of the final energy,
just as with a δ function. Thus, in the ratio of the LAAD
peaks, only the time integral remains, as can be seen
from Eq. (9), and for linear polarization the amplitude
of the nth LAAD peak is given by the generalized Bessel
function

$$J_n(a,b) = \sum_{l=-\infty}^{\infty} J_{n+2l}(a)J_l(b), \qquad (10)$$

with $a = \vec{\alpha} \cdot \vec{k}$ and $b = U_p/2\omega$. Here α is the amplitude of the periodic motion of the free electron in the linearly polarized ir dressing field. In the direction of polarization, $\alpha = A/\omega$ (in a.u.). U_p is the ponderomotive energy, ω the frequency of the ir dressing field, and $\vec{k}$ the wave vector of the electron in the dressing field.

The relative intensity of the nth LAAD peak (normalized on the zeroth peak) follows after integration over 2π solid angle $R_n = I_n/I_0$, with

$$I_n = \int J_n^2(\alpha k \cos\theta, b)\, d(\cos\theta). \qquad (11)$$

The quantity R_n will be compared with experiment.

The fit procedure described in Sec. III has been used to extract the sideband magnitude from 12 dressed spectra, taken at different intensities of the dressing field (see Fig. 8). As is the case for the theoretical data, the experimental data have been normalized on the central peak as well. The black bars represent the fitted sidebands (deconvoluted experiment), while the white bars give the predictions of the quantum-theoretical model.

The best fit to the experiment is obtained for an intensity twice the experimental one. The intensities shown in Fig. 8 correspond to the experimentally determined values. To the right of each histogram, the original spectrum is shown. As far as the relative amplitude of the sidebands is concerned, there is quite satisfactory agreement between the quantum-mechanical prediction and the experiment. We conclude that the discrepancy on the intensity is due to the uncertainty in the measurement. This shows that the approximations made in theory are quite justified and that the absorption of excess photons is due to transitions between continua after the initial ionization event.

ACKNOWLEDGMENTS

[1] H.G. Muller, P. Agostini and G. Petite, in *Atoms in Intense Laser Fields*, edited by M. Gavrila (Academic, Boston, 1992).

[2] R.R. Freeman, P.H. Bucksbaum, H. Milchberg, S. Darack, D. Schumacher, and M.E. Geusic, Phys. Rev. Lett. **59**, 1092 (1987).

[3] H.G. Muller, H.B. van Linden van den Heuvell, and M.J. van der Wiel, J. Phys. B **19**, L733 (1986).

[4] C. Leone, S. Bivona, R. Burlon, and G. Ferrante, Phys. Rev. A **38**, 5642 (1988).

[5] A. Cionga, V. Florescu, A. Maquet, and R. Taïeb, Phys. Rev. A **47**, 1830 (1993).

[6] J.M. Schins, P. Breger, P. Agostini, R.C. Constantinescu, H.G. Muller, G. Grillon, A. Antonetti, and A. Mysyrowicz, Phys. Rev. Lett. **73**, 2180 (1994).

[7] J. Tulkki, T. Aberg, A. Mantykentta, and H. Aksela, Phys. Rev. A **46**, 1357 (1992).

[8] C. Le Blanc, G. Grillon, J.P. Chambaret, A. Migus, and A. Antonetti, Opt. Lett. **18**, 140 (1993).

[9] P. Kruit and F.H. Read, J. Phys. E **16**, 313 (1983).

[10] M. Dorr and R. Shakeshaft, Phys. Rev. A **36**, 421 (1987); U. Becker *et al.*, Phys. Rev. Lett. **63**, 1054 (1989).

[11] E. Fiordilino, R. Zangara, and G. Ferrante, Phys. Rev. A **38**, 4369 (1988); R. Zangara *et al.*, Opt. Acoust. Rev. **1**, 297 (1991).

[12] H.B. van Linden van den Heuvell and H.G. Muller, in *Multiphoton Processes*, edited by S.J. Smithand and P.L. Knight (Cambridge University Press, Cambridge, 1988).

[13] W. Becker, R.R. Schlicher, and M.O. Scully, J. Phys. B **19**, L785 (1986).